PHOTONICS Research

Reducing the mode-mismatch noises in atom–light interactions via optimization of the temporal waveform

Xiaotian Feng,[1] Zhifei Yu,[1] Bing Chen,[2] Shuying Chen,[1] Yuan Wu,[1] Donghui Fan,[1] Chun-Hua Yuan,[1,5] L. Q. Chen,[1,6] Z. Y. Ou,[3] and Weiping Zhang[4]

[1]State Key Laboratory of Precision Spectroscopy, Quantum Institute for Light and Atoms, Department of Physics, East China Normal University, Shanghai 200062, China
[2]School of Electronic Science and Applied Physics, Hefei University of Technology, Hefei 230009, China
[3]Department of Physics, Indiana University-Purdue University Indianapolis, Indianapolis, Indiana 46202, USA
[4]School of Physics and Astronomy, and Tsung-Dao Lee Institute, Shanghai Jiao Tong University, Shanghai 200240, China
[5]e-mail: chyuan@phy.ecnu.edu.cn
[6]e-mail: lqchen@phy.ecnu.edu.cn

Received 22 June 2020; revised 24 August 2020; accepted 3 September 2020; posted 8 September 2020 (Doc. ID 400708); published 14 October 2020

Atom–light interface is at the core of quantum metrology and quantum information science. Associated noises during interaction processes are always inevitable and adverse. In this paper, we perform the stimulated Raman scattering (SRS) in a hot ^{87}Rb vapor cell and demonstrate the reduction of related noises originated from mode mismatch via optimizing the temporal waveform of the input seed. By using the seed with the optimized mode, the intensity fluctuation of the signal field generated in atom–light interaction is decreased by 4.3 dB. Furthermore, the fluctuation of the intensity difference between the signal and atomic spin wave is reduced by 3.1 dB. Such a temporal mode-cleaning method can be applied to improve the precision of atom interferometry using SRS and should be helpful for quantum information processing based on an atom–light correlated system.

https://doi.org/10.1364/PRJ.400708

1. INTRODUCTION

Atom–light interactions are crucial for precision measurements and quantum information processing based on the atomic systems including an atomic quantum repeater, atomic magnetometer, and atomic interferometers [1–5]. The various noises are always the limitation for the precision of measurement [6,7] and the faithfulness of quantum information [8,9]. There has been much research to reduce the noises by controlling the interaction process [10] or by utilizing the quantum states in quantum metrology [11,12]. For example, the noises of the atomic magnetometer can be suppressed below the standard quantum limit (SQL) by introducing the vacuum squeezed field and atomic squeezed state [13,14]. The phase sensitivity below the SQL of SU (1, 1) interferometers has been realized [15] by controlling the interaction processes of wave splitting and recombination. Besides, reducing the noise fluctuation of the light field and atomic system can also be helpful for the generation of the atom–light squeezed state [16,17], which is a new kind of quantum state and should be significative for quantum information processing and precision measurement based on atom–light hybrid systems.

As a promising candidate, Raman processes have been widely used in atomic quantum information processing, such as Duan-Lukin-Cirac-Zoller (DLCZ) quantum repeaters [18] and Raman quantum memory [19], and also in atomic precision measurements, e.g., the beam-splitting and recombination processes for atomic interferometers [20,21] and atom-light hybrid interferometers [17]. In Raman processes, the excess noise introduced by the spatial multimode is generally concerned. Noise reduction via spatial mode cleaning has been demonstrated [22,23]. Recently, the temporal modes of optical fields have been extensively studied to increase information capacity [24,25], to improve entanglement of two-mode squeezed light [26,27], and to give a new quantum information proposal [28]. The noise reduction in Raman scattering should be achieved by temporal mode cleaning in atom light interaction, which has not yet been reported.

In this paper, we experimentally demonstrate noise reduction by optimization of the temporal waveform. We achieve the optimized temporal mode (TM) of input Stokes light in the SRS by the iteration method. The results show that whatever the initial input Stokes waveform is, the final optimized

TMs of Stokes light are the same by iterative optimization with a fixed atomic system and a certain strong Raman pump pulse. Furthermore, the effect of the TM on the interaction noises is carefully investigated. We measure the noise fluctuation of the output Stokes field and the intensity difference between the Stokes field and the accompanied atomic spin wave, and we compare the variance data in optimized and nonoptimal cases. The intensity fluctuation of the generated Stokes field and the intensity difference decrease by 4.3 dB and 3.1 dB, respectively. Such a notable noise reduction of the Stokes field in SRS should be beneficial to improve the precision of gravity and angular velocity based on atom interferometers. Furthermore, reducing the noise fluctuation of the intensity difference indicates taking a step further toward the generation of an atom–light squeezed state, which should have a wider application in quantum information processing.

2. TEMPORAL MODE OPTIMIZATION

A. Experimental Setup

The schematic of the experimental setup to perform the SRS including the temporal waveform iteration optimizing process is shown in Fig. 1. A 5 cm long cylindrical paraffin-coated ^{87}Rb vapor cell is mounted inside a five-layer magnetic shield to reduce the stray magnetic field. The cell is operated at the temperature of 72°C. Before SRS, ~98% atoms are populated at the $|g\rangle$ level by an optical pumping (OP) pulse [generated by an additional laser, not shown in Fig. 1(a)] resonant on the $|m\rangle \rightarrow |e_2\rangle$ transition. The OP pulse is 45 μs long and 100 mW. After the OP pulse, there are two light pulses, Raman pump field W and input Stokes seed $\hat{a}_{\text{in}}$, spatially overlapping

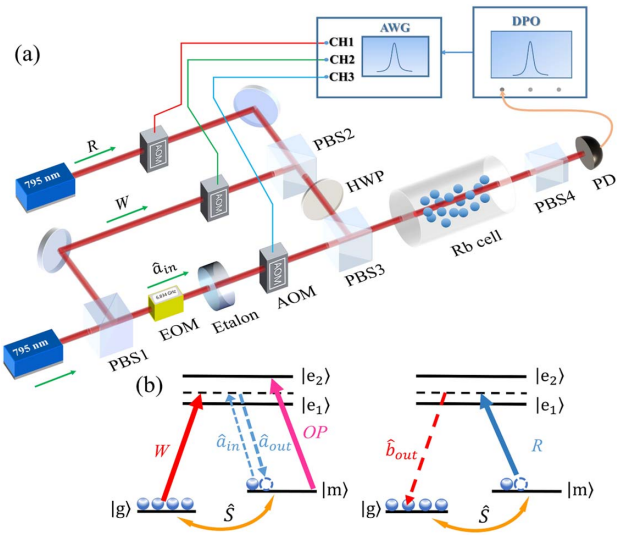

Fig. 1. (a) Schematic of the experimental setup. PBS, polarized beam splitter; HWP, half-wave plate; EOM, electro-optic modulator; AOM, acousto-optic modulator; PD, photodetector; AWG, arbitrary wave generator; DPO, digital phosphor oscilloscope. (b) Energy levels of the ^{87}Rb atom and the frequencies of the lasers: $|g, m\rangle$, hyperfine levels $|5^2S_{1/2}, F = 1, F = 2\rangle$; $|e_1, e_2\rangle$, hyperfine levels $|5^2P_{1/2}, F = 2\rangle$ and $|5^2P_{3/2}\rangle$; W, the Raman pump field; $\hat{a}_{\text{in}}$, the initial input Stokes seed; $\hat{a}_{\text{out}}$, the output Stokes field via SRS; OP, the optical pumping; $\hat{S}$, the atomic spin wave; R, the read field; $\hat{b}_{\text{out}}$, the output anti-Stokes field by the reading process.

by a polarized beam splitter (PBS) and heading into the ^{87}Rb atomic vapor together. The W laser comes from an external cavity diode laser, whose frequency is blue tuned 1.0 GHz from the $|g\rangle \rightarrow |e_1\rangle$ transition. The frequency of the $\hat{a}_{\text{in}}$ beam is red tuned to 6.8 GHz from the W laser by an electro-optic modulator (EOM, Newport model No. 4851). The temporal shapes of W and $\hat{a}_{\text{in}}$ are both adjusted by the acousto-optic modulators (AOMs), and $\hat{a}_{\text{in}}$ is then amplified to the output signal $\hat{a}_{\text{out}}$ via SRS. The output signal is detected by a photon detector (PD) after PBS4.

B. Iterative Optimization

The interaction Hamiltonian for the SRS is well known [18,29]: $\hat{H} = i\zeta\hbar\hat{a}\,\hat{S} + \text{h.c.}$, where ζ is the interaction coupling coefficient. The related input-output relationship can be written as $\hat{a}_{\text{out}} = G\hat{a}_{\text{in}} + g\hat{S}^{\dagger}_{\text{in}}$, $\hat{S}_{\text{out}} = G\hat{S}_{\text{in}} + g\hat{a}^{\dagger}_{\text{in}}$, in which G and g are gain factors and satisfy $|G|^2 - |g|^2 = 1$. In principle, the input Stokes seed ($\hat{a}_{\text{in}}$) and the amplified output Stokes field ($\hat{a}_{\text{out}}$) of the SRS can be expanded using a complete normalized orthogonal basis set $\{\Psi_k(t)\}$ of the temporal mode (TM) [30]:

$$\hat{a}_{\text{in}}(t) = \sum_{k=1}^{N} c_k \hat{a}_k \Psi_k(t) = \sum_{k=1}^{N} c_k \hat{a}_k^{(f)}(t),$$
$$\hat{a}_{\text{out}}(t) = \sum_{k=1}^{N} d_k \hat{a}_k^{(f)}(t), \tag{1}$$

where $\hat{a}_k$ is the Stokes annihilation operator for the kth-order TM, and c_k and d_k are the corresponding probability amplitudes and satisfy $\sum |c_k|^2 = \sum |d_k|^2 = 1$. To simplify the expression, we redefine the optical temporal mode operator $\hat{a}_k^{(f)}(t) = \hat{a}_k \Psi_k(t)$, whose commutation relation satisfies $\int [\hat{a}_k^{(f)}(t), \hat{a}_k^{\dagger(f)}(t)]\mathrm{d}t = \delta_{kl}$. The above basis set $\{\Psi_k(t)\}$ is related to the Raman pump field [31]. The temporal waveform of the initial Stokes field can be decomposed using $\{\Psi_k(t)\}$ with the corresponding ratio coefficients c_k. Then TMs of different orders are amplified with the corresponding gain factor G_k, which are related with the atomic optical depth, single-photon detuning, and the intensity of the Raman pump field. The final output Stokes field is the sum of all amplified TMs with the corresponding ratio coefficients d_k. It is hard to obtain the exact analytical form of the TM basis set. However, the gain factor corresponding to the lower-order TM is usually larger than that for the higher-order TM: $|G_1| > |G_2| > |G_3| > \ldots$ [32]. So after each SRS process, we should get a higher proportion of lower-order TMs and a lower proportion of higher-order TMs in $\hat{a}_{\text{out}}(t)$ compared with in $\hat{a}_{\text{in}}(t)$. Based on this, we design an iteration procedure to get the final optimized TM of the SRS.

The iterative optimization [33] is operated as shown in Fig. 2. The same waveform $\hat{a}_{\text{out}}(t)$ of the last SRS process can be used as the input seed Stokes field $\hat{a}_{\text{in}}(t)$ in the next SRS process. The output signal after SRS from the initial input $\hat{a}_{\text{in}}$ is signed as $\hat{a}^{(0)}_{\text{out}}$. The shape is recorded by an oscilloscope (Tektronix DPO7254). After that, we send the shape data to an arbitrary wave generator (AWG, Rigol DG4202), whose output drives the AOM to generate an optical signal $\hat{a}^{(1)}_{\text{in}}$ with the same pulse shape of $\hat{a}^{(0)}_{\text{out}}$. $\hat{a}^{(1)}_{\text{in}}$ acts as the input seed of Raman scattering with a next W pulse to finish the first round of iteration and

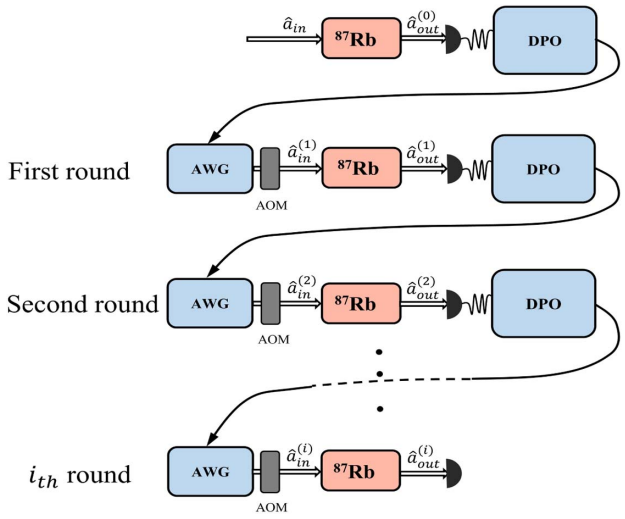

Fig. 2. Iteration diagram. $\hat{a}_{\text{in}}, \hat{a}_{\text{in}}^{(1)}, \ldots, \hat{a}_{\text{in}}^{(i)}$ are normalized initially input Stokes seeds; $\hat{a}_{\text{out}}, \hat{a}_{\text{out}}^{(1)}, \ldots, \hat{a}_{\text{out}}^{(i)}$ are output signals by SRS, corresponding to the ith iteration.

generate $\hat{a}_{\text{out}}^{(1)}$. The next round of optimization is operated based on $\hat{a}_{\text{out}}^{(1)}$. The iterative optimization keeps running until $\hat{a}_{\text{out}}^{(i)}$ is the same as $\hat{a}_{\text{in}}^{(i)}$. Finally, $\hat{a}_{\text{out}}^{(i)}$, signed as $\hat{a}_{\text{out}}^{(f)}$, is the ultimate optimized first-order TM $\hat{a}_1^{(f)}$. During the iterative operation, the W pulse and atomic system remain unchanged.

We utilize the experimental setup shown in Fig. 1 and the iteration process in Fig. 2 to obtain the first-order TM of the SRS process. The evolution from $\hat{a}_{\text{in}}$ to $\hat{a}_{\text{out}}^{(f)}$ in the iteration process is given when the W pulse is a square temporal shape with 10 μs long duration. As shown in Figs. 3(a) and 3(b), the initial $\hat{a}_{\text{in}}$ pulse consists of three Gaussian waveforms with each peak of 3 μs and four Gaussian peaks with each peak of 2 μs, respectively. The output signal gradually changes from $\hat{a}_{\text{out}}^{(0)}$ with different initial $\hat{a}_{\text{in}}$ to similar $\hat{a}_{\text{out}}^{(f)}$ with a single peak after more than five rounds of iteration. And in Fig. 3(c), we give $\hat{a}_{\text{out}}^{(f)}$ in Figs. 3(a) and 3(b) together. These two signals match very well, showing that the shape of $\hat{a}_{\text{out}}^{(f)}$ is the same whether with three or four peaks of initial $\hat{a}_{\text{in}}$. $\hat{a}_{\text{out}}^{(f)}$ is fixed with the given conditions of the Raman pump field and the atomic system.

In this paper, only the first TM is achieved through the iterative procedure. But in principle, higher-order TMs can also be picked up by subtracting the lower-order TMs in the input seed following the Gram–Schmidt process and repeating the iterative procedure. The related work has been reported in Ref. [32], where the first three orders of mutually orthogonal TMs have been experimentally characterized. Here we achieve the optimal Stokes shape with given Raman pump shape. In principle, the optimal Stokes shape is related with the Raman pump because the output Stokes field depends on the amplitude of the Raman pump in theory [31].

3. NOISE PERFORMANCE

A. Stokes Noises

Just like any other parametric amplified processes, in SRS, the gain of the Stokes field is also along with some inevitable extra noises, including quantum noises and technical noises. There has been much previous research [34–36] focused on the statistical properties of the Stokes field generated by the spontaneous Raman scattering process, among which the number of modes has also been investigated [36]. The estimation of the mode number is indeed beneficial to the experimental research. But for SRS, it is difficult to obtain the exact analytical form of $\{\Psi_k(t)\}$, and furthermore, to find the proportion of different order TMs in the output Stokes field. So here we just focus on the experimental investigation of the noise performance of the output Stokes field from SRS.

As described above, under given experimental conditions, $\hat{a}_{\text{in}}^{(f)}$ or $\hat{a}_{\text{out}}^{(f)}$ stands for the optimized TM of SRS, which should correspond to the larger gain factor as a result of the better mode match between the interaction system and the input Stokes seed [32]. As a comparison, the input seed of the arbitrary temporal waveform consists of different order TMs that are orthogonal with each other. Since the stimulated amplification of each order by SRS is not relevant to the other orders, and the final output signal is the sum of all modes, it may cause significant intensity fluctuation of the output signal to limit the measurement precision. For example, for atomic interferometers using SRS as beam-splitting and recombination processes, the intensity fluctuation of the output signal is certain to cause the instability of the wave-splitting ratio. In the respect of quantum noise alone, the larger gain effect also brings in more

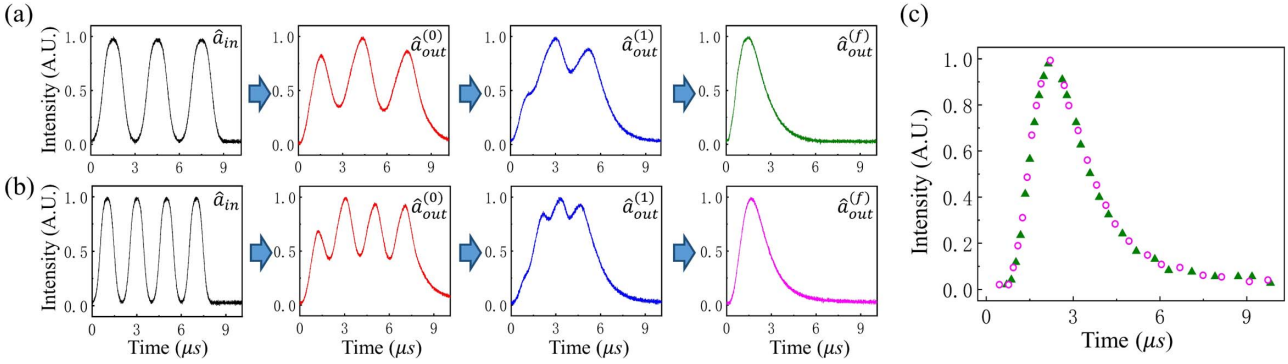

Fig. 3. (a) and (b) $\hat{a}_{\text{in}}$ is the initially input seed waveform and $\hat{a}_{\text{out}}^{(0)}$ is the corresponding output signal of SRS. $\hat{a}_{\text{out}}^{(1)}$ is the output signal of SRS in the first round, $\hat{a}_{\text{out}}^{(1)}$ is stable waveform after several iteration rounds. (c) Pink circles and green solid triangles are $\hat{a}_{\text{out}}^{(f)}$ corresponding to different $\hat{a}_{\text{in}}$ in (a) and (b), respectively.

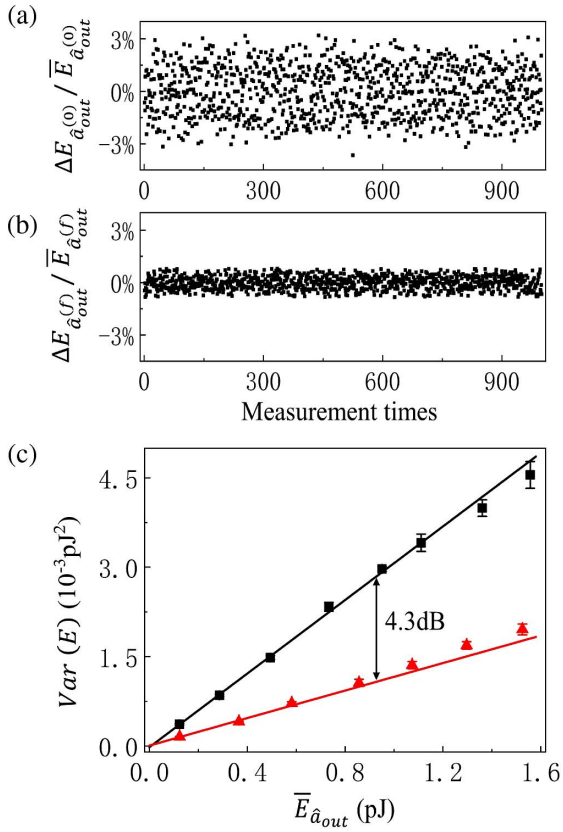

Fig. 4. (a) and (b) The different energy fluctuations $\Delta E_{\hat{a}_{\rm out}^{(0)}}$ of $\hat{a}_{\rm out}^{(0)}$ and $\Delta E_{\hat{a}_{\rm out}^{(f)}}$ of $\hat{a}_{\rm out}^{(f)}$ during many measurement times. (c) $\overline{E}_{\hat{a}_{\rm out}}$ is the average energy of the output Stokes field. Black square and red triangle curves are respective Var(E) for $E_{\hat{a}_{\rm out}^{(0)}}$ and $E_{\hat{a}_{\rm out}^{(f)}}$ both with 100 ns long square-W pulse.

associated noises [37]. However, as shown below, our experimental results show that the output Stokes noise is actually suppressed in the case of an optimized Stokes seed corresponding to the larger gain factor compared with the nonoptimal case. So the 4.3 dB improvement in Fig. 4(c) is not due to the reduction of quantum fluctuation. It should be caused by some technical noise. And here we believe that it is mainly due to the imperfect intensity modulation introduced by the AOM. This can be understood by considering the more complex temporal structure of the higher-order TMs in the Stokes seed, which results in the unstable response during the intensity modulation process inside the AOM and is further amplified through the SRS.

To test the noise reducing effect of temporal mode selection, we experimentally measure the intensity variance of $\hat{a}_{\rm out}^{(0)}$ with the nonoptimal square Stokes seed $\hat{a}_{\rm in}$ and $\hat{a}_{\rm out}^{(f)}$ with the optimized TM $\hat{a}_{\rm in}^{(f)}$ obtained in the iteration procedure. We record more than 10^3 sets of single output signal using an oscilloscope, and then obtain the pulse energy data E by integrating each shot. The data in cases of $\hat{a}_{\rm out}^{(0)}$ and $\hat{a}_{\rm out}^{(f)}$ are given in Figs. 4(a) and 4(b). The average energies in single $\hat{a}_{\rm out}^{(0)}$ and $\hat{a}_{\rm out}^{(f)}$ are equal by carefully adjusting the intensity of $\hat{a}_{in}$ and $\hat{a}_{\rm in}^{(f)}$. It is obvious that the intensity fluctuation of $\hat{a}_{\rm out}^{(0)}$ is much larger than that of $\hat{a}_{\rm out}^{(f)}$. The variance of energy data can be calculated via $\mathrm{Var}(E) = \overline{(\Delta E)^2} = \overline{(E - \overline{E})^2}$. The measured variances for $\hat{a}_{\rm out}^{(0)}$ and $\hat{a}_{\rm out}^{(f)}$ both in square-shape W pulses are given in Fig. 4(c). Solid lines are fitted using linear function, and the variance for optimized $\hat{a}_{\rm out}^{(f)}$ is decreased by 4.3 dB compared to that of nonoptimal $\hat{a}_{\rm out}^{(0)}$.

In atom interferometers, the beam splitting for the atomic waves is operated by an SRS process. The intensity fluctuation of the amplified Stokes field causes the number fluctuation of the atomic waves, given the general expression of the phase sensitivity [38] $\Delta\phi = \frac{[\mathrm{Var}(N)]^{1/2}}{|\partial\langle\hat{N}\rangle/\partial\phi|}$. So in principle, the noise reduction of 4.3 dB (~2.6 times) in the output Stokes field will result in about 2.2 dB (~1.3 times) improvement of the phase sensitivity.

B. Intensity Difference Noises

In Raman scattering, generation of $\hat{a}_{\rm out}$ always accompanies with atomic spin wave $\hat{S}$ as shown in Fig. 1. On the ideal condition, the photon number of $\hat{a}_{\rm out}$ should be equal to $\hat{S}$, that is, $\hat{a}_{\rm out}$ and $\hat{S}$ bring into being an atom–light two-mode squeezed state, which is a new source of squeezed states and can be applied to improve precision measurement [13,14,39]. In the above, we have shown the intensity variance of the output Stokes field can be decreased by the optimized TM seed. As for applications, the inherent intensity correlation between $\hat{a}_{\rm out}$ and $\hat{S}$ is also very promising and useful [40]. However, there always exist some mechanisms causing extra noises in the real experiments, such as spatial and temporal multimodes, resonant absorption processes, optical loss, and atomic decoherence. The effect of the spatial multimode has been demonstrated, where the intensity fluctuations between $\hat{a}_{\rm out}$ and $\hat{S}$ are significantly decreased via coherent feedback [22] to achieve a pure first-order spatial mode. Here we focus on the effect of temporal modes on the fluctuation of intensity difference.

Different from the Stokes noise discussed in Section 3.A, the measurement of the intensity difference can avoid the influence of technical noise to a certain extent, which allows us to focus on the quantum fluctuations during the SRS process. In order to intuitively understand the noise suppression effect in theory, we may as well take the ideal case that the atomic spin wave $\hat{S}$ can be perfectly transformed back into the optical field $\hat{b}_{\rm out}$, and we denote the intensity difference operator as $\hat{I}_- = \hat{a}_{\rm out}^{\dagger}\hat{a}_{\rm out} - \hat{b}_{\rm out}^{\dagger}\hat{b}_{\rm out}$. According to the input-output relationship of SRS process, it is easy to check out that the intensity difference variance can be expressed as

$$\mathrm{Var}_{\rm ideal}(I_-) = I_{\rm in} = I_{\rm out}/|G|^2, \tag{2}$$

where $I_{\rm in}$ and $I_{\rm out}$ are respectively the intensity of the input Stokes seed and the amplified output Stokes field. As discussed in Section 2.B, the gain factors for lower TMs are usually larger than those for the higher TMs: $G_i > G_j\,(i < j)$. On the condition of the same output Stokes intensity in the SRS, the needed input Stokes seed intensity is the smallest for the first-order TM and thus corresponds to the lowest intensity difference variance.

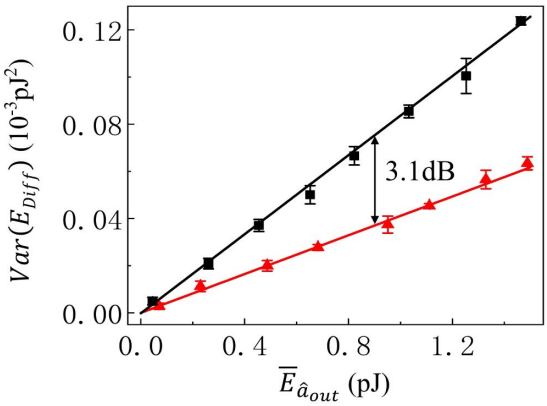

Fig. 5. Black square and red triangle curves are respective Var(E_{Diff}) for $\hat{a}_{\mathrm{out}}^{(0)}$ and $\hat{a}_{\mathrm{out}}^{(f)}$ both with the square-W and square-R pulse acquired in the experiment.

To experimentally measure the intensity difference, a strong 100 ns long read pulse (R) is sent into the atomic system after the generation of $\hat{a}_{\mathrm{out}}$. The frequency of the read laser is red detuned 1.0 GHz from the atomic transition $|m\rangle \rightarrow |e_1\rangle$. The read pulse retrieves the atomic spin wave $\hat{S}$ back into an optical signal $\hat{b}_{\mathrm{out}}$. In an atomic vapor cell, the atomic decoherence is mainly due to atoms flying out of the interaction region. To retrieve an $\hat{S}$ as large as possible, the W pulse is turned on just for 100 ns. The delay between W and R is 50 ns. $\hat{a}_{\mathrm{out}}$ and $\hat{b}_{\mathrm{out}}$ pass the same path. We record $\hat{a}_{\mathrm{out}}$ and $\hat{b}_{\mathrm{out}}$ in each cycle. The measured retrieved efficiency η_R is 70%. $\overline{E}_{\hat{a}_{\mathrm{out}}}$, $\overline{E}_{\hat{b}_{\mathrm{out}}}$ are the average energies of $\hat{a}_{\mathrm{out}}$, $\hat{b}_{\mathrm{out}}$, respectively.

Under the certain W and $\hat{a}_{\mathrm{in}}^{(f)}$, we record 10^4 sets of $\hat{a}_{\mathrm{out}}$ and $\hat{b}_{\mathrm{out}}$, and we take $E_{\mathrm{Diff}} = E_{\hat{a}_{\mathrm{out}}} - E_{\hat{b}_{\mathrm{out}}}/\eta_R$ in each cycle as the intensity difference between $\hat{a}_{\mathrm{out}}$ and $\hat{b}_{\mathrm{out}}$. Then a series of the variance of E_{Diff}, Var(E_{Diff}) can be acquired by changing the intensity of the input seed. The results are plotted in Fig. 5 with $\overline{E}_{\hat{a}_{\mathrm{out}}}$ as the x axis and Var(E_{Diff}) as the y axis. The experiment data is fitted using linear function and the slope k of the fitted line represents the magnitude of the intensity difference noise. The slope k for $\hat{a}_{\mathrm{out}}$ with square-W and square-R pulses (black square curve) is 8.38×10^{-5} and can be reduced to 4.11×10^{-5} (red triangle curve) with $\hat{a}_{\mathrm{out}}^{(f)}$. This means through the temporal waveform optimization of the seed Stokes field, we can get 3.1 dB noise reduction for the intensity difference between the output Stokes field and anti-Stokes field.

4. CONCLUSION

In this paper, we demonstrate the reduction of mode-mismatch noises in atom–light interactions by temporal mode cleaning. The first-order temporal mode is achieved by the iteration method, which depends on the Raman pump shape whatever the input seed is. By using the optimized temporal mode, the noise fluctuation of the output signal decreases by 4.3 dB compared with the nonoptimal case. Meanwhile, the noise fluctuation of the intensity difference between the signal and atomic spin wave is reduced by 3.1 dB. Our results show that the temporal multimode, similar with the spatial multimode, also contributes significant noises into the measurements based on atomic systems. This point has always been ignored in previous research. Our results can also be applied to crystal systems [41,42] and should be helpful to improve the precision of atomic measurement and to achieve the atom–light squeezed state.

Funding. National Key Research and Development Program of China (2016YFA0302001); National Natural Science Foundation of China (11874152, 11974111, 11604069, 11654005, 91536114); Natural Science Foundation of Shanghai (17ZR1442800); Fundamental Research Funds for the Central Universities; Shanghai Municipal Science and Technology Major Project (2019SHZDZX01).

Disclosures. The authors declare no conflicts of interest.

REFERENCES

1. H. J. Kimble, "The quantum internet," Nature **453**, 1023–1030 (2008).
2. Z.-S. Yuan, Y.-A. Chen, B. Zhao, S. Chen, J. Schmiedmayer, and J.-W. Pan, "Experimental demonstration of a BDCZ quantum repeater node," Nature **454**, 1098–1101 (2008).
3. N. Sangouard, C. Simon, H. De Riedmatten, and N. Gisin, "Quantum repeaters based on atomic ensembles and linear optics," Rev. Mod. Phys. **83**, 33–80 (2011).
4. P. Berg, S. Abend, G. Tackmann, C. Schubert, E. Giese, W. Schleich, F. Narducci, W. Ertmer, and E. Rasel, "Composite-light-pulse technique for high-precision atom interferometry," Phys. Rev. Lett. **114**, 063002 (2015).
5. G. Bao, S. Wu, S. Liu, W. Huang, Z. Li, L. Chen, C.-H. Yuan, and W. Zhang, "Enhancement of the signal-to-noise ratio of an atomic magnetometer by 10 dB," Phys. Rev. Appl. **11**, 054075 (2019).
6. J. Geremia, J. K. Stockton, and H. Mabuchi, "Suppression of spin projection noise in broadband atomic magnetometry," Phys. Rev. Lett. **94**, 203002 (2005).
7. M. Koschorreck, M. Napolitano, B. Dubost, and M. Mitchell, "Sub-projection-noise sensitivity in broadband atomic magnetometry," Phys. Rev. Lett. **104**, 093602 (2010).
8. J. Appel, E. Figueroa, D. Korystov, M. Lobino, and A. Lvovsky, "Quantum memory for squeezed light," Phys. Rev. Lett. **100**, 093602 (2008).
9. M. Lobino, C. Kupchak, E. Figueroa, and A. Lvovsky, "Memory for light as a quantum process," Phys. Rev. Lett. **102**, 203601 (2009).
10. F. Hudelist, J. Kong, C. Liu, J. Jing, Z. Ou, and W. Zhang, "Quantum metrology with parametric amplifier-based photon correlation interferometers," Nat. Commun. **5**, 3049 (2014).
11. C. M. Caves, "Quantum-mechanical noise in an interferometer," Phys. Rev. D **23**, 1693–1708 (1981).
12. Y. Ma, H. Miao, B. H. Pang, M. Evans, C. Zhao, J. Harms, R. Schnabel, and Y. Chen, "Proposal for gravitational-wave detection beyond the standard quantum limit through EPR entanglement," Nat. Phys. **13**, 776–780 (2017).
13. F. Wolfgramm, A. Cere, F. A. Beduini, A. Predojević, M. Koschorreck, and M. W. Mitchell, "Squeezed-light optical magnetometry," Phys. Rev. Lett. **105**, 053601 (2010).
14. W. Wasilewski, K. Jensen, H. Krauter, J. J. Renema, M. Balabas, and E. S. Polzik, "Quantum noise limited and entanglement-assisted magnetometry," Phys. Rev. Lett. **104**, 133601 (2010).
15. W. Du, J. Jia, J. Chen, Z. Ou, and W. Zhang, "Absolute sensitivity of phase measurement in an SU(1, 1) type interferometer," Opt. Lett. **43**, 1051–1054 (2018).
16. W. Wasilewski, T. Fernholz, K. Jensen, L. Madsen, H. Krauter, C. Muschik, and E. S. Polzik, "Generation of two-mode squeezed and entangled light in a single temporal and spatial mode," Opt. Express **17**, 14444–14457 (2009).

17. B. Chen, C. Qiu, S. Chen, J. Guo, L. Chen, Z. Ou, and W. Zhang, "Atom-light hybrid interferometer," Phys. Rev. Lett. **115**, 043602 (2015).
18. L.-M. Duan, M. Lukin, J. I. Cirac, and P. Zoller, "Long-distance quantum communication with atomic ensembles and linear optics," Nature **414**, 413–418 (2001).
19. K. Reim, J. Nunn, V. Lorenz, B. Sussman, K. Lee, N. Langford, D. Jaksch, and I. Walmsley, "Towards high-speed optical quantum memories," Nat. Photonics **4**, 218–221 (2010).
20. T. Gustavson, P. Bouyer, and M. Kasevich, "Precision rotation measurements with an atom interferometer gyroscope," Phys. Rev. Lett. **78**, 2046–2049 (1997).
21. L. Zhou, S. Long, B. Tang, X. Chen, F. Gao, W. Peng, W. Duan, J. Zhong, Z. Xiong, J. Wang, and M. Zhan, "Test of equivalence principle at 10^{-8} level by a dual-species double-diffraction Raman atom interferometer," Phys. Rev. Lett. **115**, 013004 (2015).
22. J. Guo, L. Chen, P. Yang, Z. Li, Y. Wu, X. Feng, C.-H. Yuan, Z. Ou, and W. Zhang, "88% conversion efficiency with an atomic spin wave mediated mode selection," Opt. Lett. **42**, 1752–1755 (2017).
23. X.-H. Bao, A. Reingruber, P. Dietrich, J. Rui, A. Dück, T. Strassel, L. Li, N.-L. Liu, B. Zhao, and J.-W. Pan, "Efficient and long-lived quantum memory with cold atoms inside a ring cavity," Nat. Phys. **8**, 517–521 (2012).
24. I. Usmani, M. Afzelius, H. De Riedmatten, and N. Gisin, "Mapping multiple photonic qubits into and out of one solid-state atomic ensemble," Nat. Commun. **1**, 12 (2010).
25. M. Bonarota, J. Le Gouët, and T. Chaneliere, "Highly multimode storage in a crystal," New J. Phys. **13**, 013013 (2011).
26. X. Guo, N. Liu, X. Li, and Z. Ou, "Complete temporal mode analysis in pulse-pumped fiber-optical parametric amplifier for continuous variable entanglement generation," Opt. Express **23**, 29369–29383 (2015).
27. J. Li, Y. Liu, N. Huo, L. Cui, C. Feng, Z. Ou, and X. Li, "Pulsed entanglement measured by parametric amplifier assisted homodyne detection," Opt. Express **27**, 30552–30562 (2019).
28. B. Brecht, D. V. Reddy, C. Silberhorn, and M. Raymer, "Photon temporal modes: a complete framework for quantum information science," Phys. Rev. X **5**, 041017 (2015).
29. K. Hammerer, A. S. Sørensen, and E. S. Polzik, "Quantum interface between light and atomic ensembles," Rev. Mod. Phys. **82**, 1041 (2010).
30. M. Raymer, Z. Li, and I. Walmsley, "Temporal quantum fluctuations in stimulated Raman scattering: coherent-modes description," Phys. Rev. Lett. **63**, 1586–1589 (1989).
31. M. Raymer, I. Walmsley, J. Mostowski, and B. Sobolewska, "Quantum theory of spatial and temporal coherence properties of stimulated Raman scattering," Phys. Rev. A **32**, 332–344 (1985).
32. N. Huo, Y. Liu, J. Li, L. Cui, X. Chen, R. Palivela, T. Xie, X. Li, and Z. Ou, "Direct temporal mode measurement for the characterization of temporally multiplexed high dimensional quantum entanglement in continuous variables," Phys. Rev. Lett. **124**, 213603 (2020).
33. I. Novikova, A. V. Gorshkov, D. F. Phillips, A. S. Sørensen, M. D. Lukin, and R. L. Walsworth, "Optimal control of light pulse storage and retrieval," Phys. Rev. Lett. **98**, 243602 (2007).
34. I. A. Walmsley and M. G. Raymer, "Observation of macroscopic quantum fluctuations in stimulated Raman scattering," Phys. Rev. Lett. **50**, 962–965 (1983).
35. S. J. Kuo, D. T. Smithey, and M. G. Raymer, "Spatial interference of macroscopic light fields from independent Raman sources," Phys. Rev. A **43**, 4083–4086 (1991).
36. M. Parniak, A. Leszczyński, and W. Wasilewski, "Coupling of four-wave mixing and Raman scattering by ground-state atomic coherence," Phys. Rev. A **93**, 053821 (2016).
37. C. M. Caves, "Quantum limits on noise in linear amplifiers," Phys. Rev. D **26**, 1817–1839 (1982).
38. M. O. Scully and J. P. Dowling, "Quantum-noise limits to matter-wave interferometry," Phys. Rev. A **48**, 3186–3190 (1993).
39. M. Tse, H. Yu, N. Kijbunchoo, A. Fernandez-Galiana, P. Dupej, L. Barsotti, C. Blair, D. Brown, S. Dwyer, and A. Effler, "Quantum-enhanced advanced LIGO detectors in the era of gravitational-wave astronomy," Phys. Rev. Lett. **123**, 231107 (2019).
40. C. H. van der Wal, M. D. Eisaman, A. André, R. L. Walsworth, D. F. Phillips, A. S. Zibrov, and M. D. Lukin, "Atomic memory for correlated photon states," Science **301**, 196–200 (2003).
41. M. F. Yanik, W. Suh, Z. Wang, and S. Fan, "Stopping light in a waveguide with an all-optical analog of electromagnetically induced transparency," Phys. Rev. Lett. **93**, 233903 (2004).
42. P. Sharapova, A. M. Pérez, O. V. Tikhonova, and M. V. Chekhova, "Schmidt modes in the angular spectrum of bright squeezed vacuum," Phys. Rev. A **91**, 043816 (2015).